Precision Resonance Scans at $\overline{\text{P}}$ANDA

Iman Keshk on behalf of the $\overline{\text{P}}$ANDA Collaboration

Institute for Experimental Physics I, Ruhr University Bochum, Germany

E-mail: `ikeshk@ep1.rub.de`

Abstract. Due to a high antiproton beam resolution the $\overline{\text{P}}$ANDA experiment at FAIR will offer a unique possibility to perform precise resonance energy scans. Thereby a precise line shape and width measurement of very narrow resonances like the charmonium-like $X(3872)$, which is discussed to be exotic, becomes feasible. Monte Carlo studies have been performed, to address the achievable sensitivities of such measurements, assuming different signal cross-sections, line shapes and luminosity combinations.

1. Introduction

Besides conventional charmonium states ($c\bar{c}$) in the last decades many charmonium-like states have been observed by different experiments. The so-called XYZ states show characteristics different from conventional charmonia and unusual decay modes, which is why they are discussed to be of exotic nature. Although various theoretical interpretations of these states exist (molecular states, hybrids, multi-quark states, threshold enhancements etc.), the underlying nature remains unclear until now. A more detailed description of the so-called XYZ puzzle can be found in [1]. The first discovered charmonium-like state was the $X(3872)$, observed by the Belle Collaboration in 2003 in the reaction $B^{\pm} \to K^{\pm} X(3872) \to K^{\pm} \pi^+ \pi^- J/\psi$ [2]. The observation was confirmed by other experiments like LHCb, where an amplitude analysis revealed the quantum numbers $J^{PC} = 1^{++}$ [3]. One particular feature of the $X(3872)$ is that its measured mass is indistinguishable from the DD^* threshold, moreover it is not even clear, if it lies above or below the threshold. Since the di-pion system in $X(3872) \to J/\psi \pi^+ \pi^-$ is originating from $\rho^0(770)$ decays [4], the reaction $X(3872) \to \rho^0(770) J/\psi$ is strongly isospin breaking, which emphasises once again a possible underlying exotic nature. To reveal the nature of this state and distinguish between theoretical interpretations a precise line shape and width measurement must be carried out. Previous width measurements, which determined an experimental upper limit of $1.2\,\text{MeV}$ at 90% confidence level [5] were limited by the respective detector resolution. The $\overline{\text{P}}$ANDA experiment offers the unique opportunity for such precise measurements by performing a resonance scan, which will not be limited by the detector resolution but by the remarkable high resolution of the antiproton beam.

2. Resonance Energy Scans with $\overline{\text{P}}$ANDA

2.1. The $\overline{\text{P}}$ANDA Experiment

The $\overline{\text{P}}$ANDA experiment, which is currently under construction, will be located at the future accelerator complex FAIR at GSI, Germany [6]. It aims to improve the knowledge of strong interactions in the non-perturbative regime and hadron structure, by studying antiproton-proton

annihilations. The $\overline{\text{P}}$ANDA multi-purpose detector is a fixed-target spectrometer, which will be located at the High Energy Storage Ring (HESR). The HESR will deliver an antiproton beam with momenta between $1.5\,\text{GeV}/c$ and $15\,\text{GeV}/c$ hitting a high density fixed target of either a cluster-jet or a frozen hydrogen pellet type. Consisting of a target spectrometer and a forward spectrometer, which covers polar angles below 10 and 5 degrees in the horizontal and vertical plane, the detector achieves a solid angle coverage of almost 4π, while the numerous subdetectors ensure a proper reconstruction of both charged and neutral particles.

2.2. Resonance Energy Scan of the $X(3872)$
For the performance of a resonance energy scan, the cross-section of the formation process $\overline{p}p \to X(3872) \to J/\psi\pi^+\pi^-$ will be determined at different center-of-mass energies by adjusting the beam momentum as shown in fig. 1a. By unfolding the beam energy profile, which must be precisely known, the energy dependent cross-section can be determined from the experimentally observed event yield per scan point. The integrated luminosity $\mathcal{L}$ and the beam resolution dp/p are therefore of particular importance. In the performed sensitivity studies three different scenarios were taken into account, based on three different phases of the accelerator completion. The characteristics of the expected High Luminosity (HL) mode of the final accelerator set up, the High Resolution (HR) mode and the "Phase-1" (P1) mode of the initial set up are collected in table 1.

The natural decay width Γ_0 of the $X(3872)$ will be measured for different HESR operation modes by fitting a Voigt function, a convolution of a Breit-Wigner with a width Γ_0 and a Gaussian with a standard deviation σ_{Beam} accounting for the spread in beam momentum. Besides the determination of the natural width in the case of a Breit-Wigner line shape, a second scenario is considered, assuming the $X(3872)$ to be a loosley bound $(D\overline{D}^*)^0$ molecule or a virtual scattering state created by threshold dynamics. In this case, the Flatté parameter E_f [8] is used, to determine the nature of being a bound or a virtual state, see fig. 1b. States with E_f below the threshold energy of $E_{th} = -8.5652\,\text{MeV}$ are considered as bound, while states with E_f above E_{th} are regarded as virtual states. In the present studies [7] the sensitivity will be investigated, to distinguish between the two natures taking E_f into account. Fig. 1c and 1d show the line shape in case of a Breit-Wigner resonance and for the molecule scenario for specific values of Γ_0 and E_f respectively.

Table 1: Beam resolution dp/p and integrated luminosities $\mathcal{L}$ of the three different HESR operation modes [7].

HESR mode	dp/p	$\mathcal{L}[1/(\text{day} \cdot \text{nb})]$
P1	$5 \cdot 10^{-5}$	1170
HL	$1 \cdot 10^{-4}$	13680
HR	$2 \cdot 10^{-5}$	1368

3. Event Simulation and Reconstruction
A detailed description of the event simulation and reconstruction, performed within the PandaRoot software framework can be found in [7]. The Monte Carlo data for the two signal channels $\overline{p}p \to X(3872) \to J/\psi\rho^0 \to e^+e^-\pi^+\pi^-$ and $\overline{p}p \to X(3872) \to J/\psi\rho^0 \to \mu^+\mu^-\pi^+\pi^-$, the non-resonant reactions $\overline{p}p \to J/\psi\pi^+\pi^- \to e^+e^-\pi^+\pi^-$ and $\overline{p}p \to J/\psi\pi^+\pi^- \to \mu^+\mu^-\pi^+\pi^-$
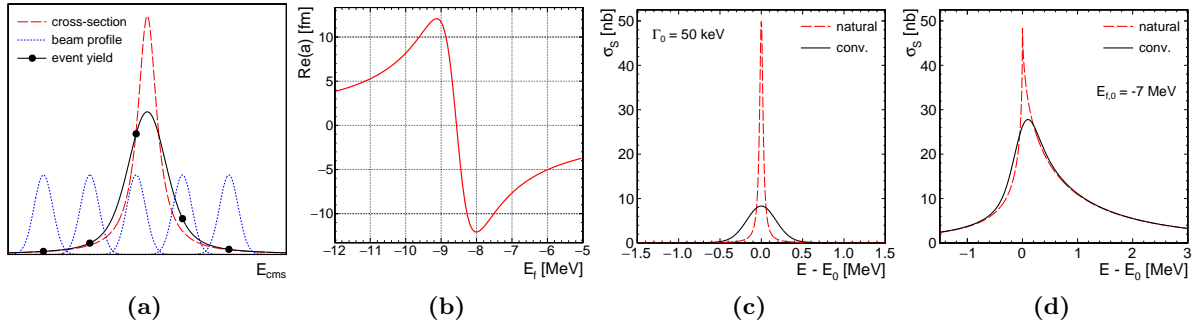
Figure 1: Schematic of a resonance energy scan (a), the functional dependence of the real part of the scattering length on the parameter E_f (b) and two examples for different line shapes in case of a Breit-Wigner resonance (c) and a virtual state (d) [7].

and for the generic background data samples are taken at a center-of-mass energy of $E_{cms} = 3872$ MeV. Since the energy-scan window only ranges up to a few MeV it is assumed, that the reconstruction efficiency does not vary much for each scan point. After a proper event selection and comprehensive background studies reconstruction efficiencies of $\epsilon_S = 12.2\%$ in case of the J/ψ decaying to e^+e^- and $\epsilon_S = 15.2\%$ in case of the decay to $\mu^+\mu^-$ are obtained. Fig. 2 shows the invariant di-lepton masses after the final selection. The generic background could be almost completely suppressed while the non-resonant background is still producing structures at the mass of the J/ψ.

## 4. Simulation of the Resonance Energy Scan of the $X(3872)$

The parameters of interest as input for the simulation of a resonance energy scan are the corresponding reconstruction efficiency ϵ_i, the integrated luminosity $\mathcal{L}_i$ at each scan point $E_{cms,i}$ and the effective cross-section $\sigma^*(E_{cms,i})$. With the product f_b of all involved branching fractions of the reconstructed decay the expected signal yield can then be described as

$$N_i = \sigma^*(E_{cms,i}) \cdot \epsilon_i \cdot \mathcal{L}_i \cdot f_b. \tag{1}$$

The resonance energy scan was simulated for different widths Γ_0 in case of a Breit-Wigner resonance scenario and different Flatté parameters E_f in case of a molecular scenario. Since the scan procedure is not limited to the scan of the $X(3872)$ with an assumed signal cross section of 50 nb [7], further signal cross sections were taken into account, as a prognosis for other resonance scans.
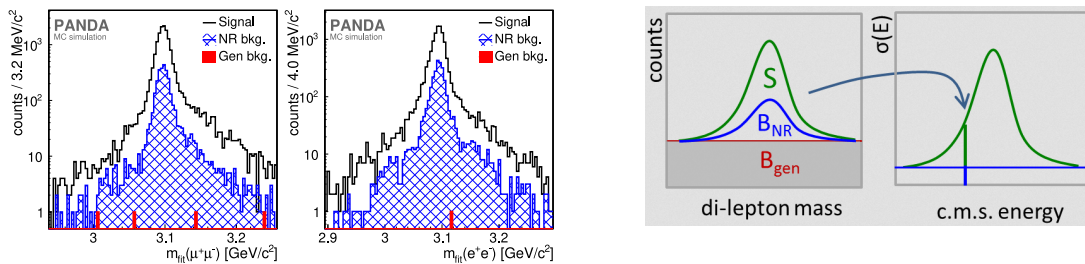
Figure 2: Invariant di-lepton mass after the final selection (left) and scheme of extracting the event yield for each scan point (right) [7].
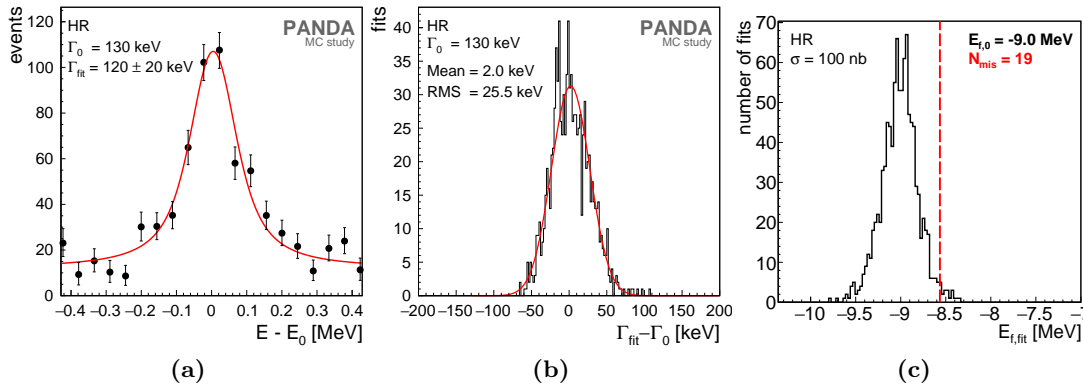
Figure 3: Energy dependent yield distribution (a), distribution of the extracted widths compared to the input value for 1000 toy MC experiments (b) and misidentification fraction for the molecular case (c). [7].

The event yield of the J/ψ in the di-lepton mass was fitted and extracted for each scan point, so that the generic background is removed and the non-resonant background is kept as a constant contribution below the $X(3872)$ signal (fig. 2 (right)). The resultant energy-dependent yield distribution is shown exemplarily for $\sigma_S = 100\,\text{nb}$ and $\Gamma_0 = 130\,\text{keV}$ in fig. 3a. The extracted width of $120\pm20\,\text{keV}$ is in good agreement with the generated width. Fig. 3b shows the extracted width compared to the generated one for 1000 toy MC experiments allowing to determine the precision and the accuracy by identifying the root-mean-square (RMS) and the shift of the distribution. The obtained sensitivities for the Breit-Wigner scenario are shown in fig. 4a and 4b and as a function of the input width for two different assumed cross sections. It can be seen, that the larger the input width and the signal cross-section, the higher is the precision of the measurement for all three HESR modes. While up to $\Gamma_0 = 200\,\text{keV}$ the HR mode shows the best performance, for input width above the HL mode is superior.

For the molecule scenario the precision of the measurement is based on the misidentification probability of the nature of the state. It is defined by the amount of MC scans extracting a Flatté parameter which misidentifies the nature as a bound state, when it was generated as a virtual state or vice-versa, as it is shown in fig. 3c for an input parameter of $E_f = -9\,\text{MeV}$. The misidentification probability P_mis for two different signal cross-sections as a function of the input E_f is shown in fig. 4c and 4d. As expected, the closer E_f is to the threshold energy, the higher P_mis gets, while the HL operation mode is superior throughout the complete range. For both scenarios a total scan time of 80 days is assumed, taking 40 scan points into account. A detailed description of the treatment of systematic uncertainties can be found in [7].

5. Summary and Outlook

Due to the remarkable resolution of the antiproton beam, the $\overline{\text{P}}$ANDA experiment offers the unique possibility to perform precise width and line shape measurements which are not limited by the detector resolution. Since for the width of the $X(3872)$ only an upper limit of $1.2\,\text{MeV}$ exists so far, a measurement with sub MeV resolution is required to get a better understanding of the nature of this charmonium-like state. A 3σ sensitivity ($\Delta\Gamma_\text{meas}/\Gamma_\text{meas} = 33\%$ precision) can be obtained for a natural decay width larger than $40\,\text{keV}$ with the HR mode in case of a Breit-Wigner resonance. The P1 mode of the initial accelerator setup achieves a 3σ precision for natural widths larger than $110\,\text{keV}$. In case of a molecular state a 90% probability for a correct identification as a bound or a virtual state was achieved for a Flatté parameter with a distance
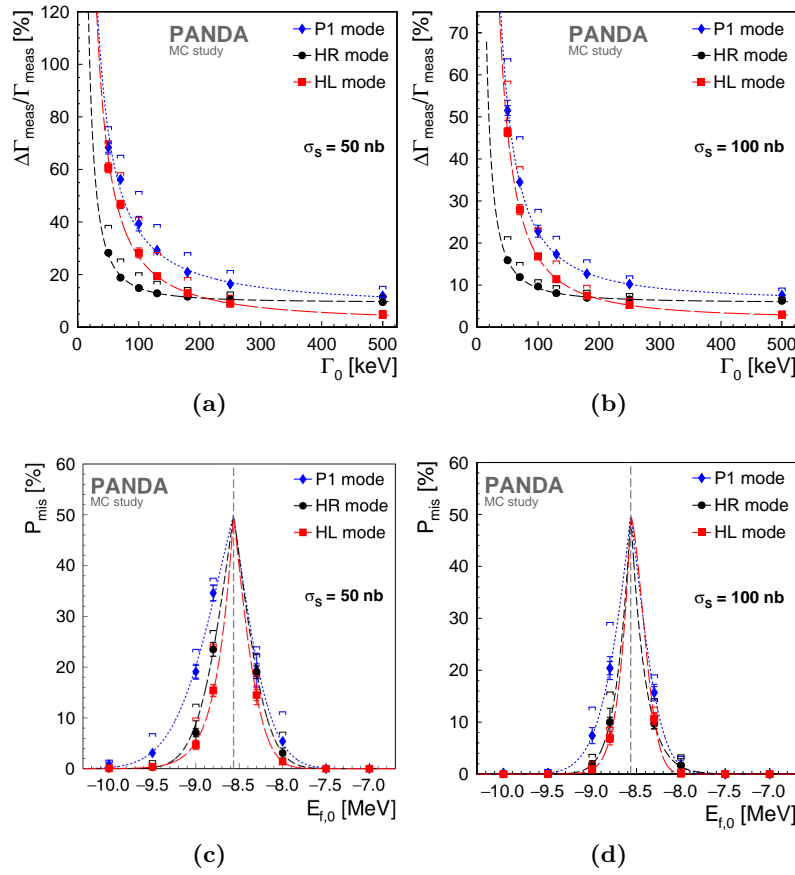
Figure 4: Sensitivity measurements for the Breit-Wigner case study (a)(b) and for the molecule case study (c)(d) for signal cross-sections of $50\,\mathrm{nb}$ and $100\,\mathrm{nb}$. The inner error bars represent the statistical and the outer ones the systematic errors. [7].

larger than $300\,\mathrm{keV}$ to the threshold energy for the HL mode and larger than $700\,\mathrm{keV}$ for the P1 mode.

The performance of a resonance energy scan is not limited to this specific case and can be used to analyse more reactions of interest, like $\bar{p}p \to \phi\phi$, as tensor resonances were observed in the $\phi\phi$ system [9][10][11] in the same region where Lattice QCD calculations predict the existence of the tensor glueball [12].

References

[1] Olsen S L, Skwarnicki T and Zieminska D 2018 *Rev. Mod. Phys.* **90** 015003
[2] Choi S K *et al.* (BELLE Collaboration) 2003 *Phys. Rev. Lett.* **91** 262001
[3] Aaij R *et al.* (LHCb Collaboration) 2013 *Eur. Phys. J.* C **73** 2462
[4] Abulencia A *et al.* (CDF Collaboration) 2006 *Phys. Rev. Lett.* **96** 102002
[5] Choi S K *et al.* (BELLE Collaboration) 2011 *Phys. Rev.* D **84** 052004
[6] Erni W *et al.* (PANDA Collaboration) 2009 arXiv:0903.3905 [hep-ex]
[7] Barucca G *et al.* (PANDA Collaboration) 2019 *Eur. Phys. J.* A **55:** 42
[8] Kalashnikova Yu S *et al.* 2010 *Phys. Atom. Nucl.* **73** 1592
[9] Evangelista C *et al.* (JETSET Collaboration) 1998 *Phys. Rev.* D **57** 5370
[10] Ablikim M *et al.* (BESIII Collaboration) 2011 *Phys. Rev.* D **93** 112011
[11] Etkin A *et al.* (BNL Laboratory) 1988 *Phys. Lett.* B **201** 568-572
[12] Chen Y *et al.* 2005 *Phys. Rev.* D **73** 014526